JOURNAL OF SYNCHROTRON RADIATION

ISSN 1600-5775

Development of an undulator with a variable magnetic field profile

Takashi Tanaka,[a]* Yuichiro Kida,[a] Ryota Kinjo,[a] Tadashi Togashi,[a,b] Hiromitsu Tomizawa,[a,b] Satoshi Hashimoto,[c] Shuji Miyamoto,[c] Sumiyuki Okabe[d] and Yoshihito Tanaka[d]

[a]RIKEN SPring-8 Center, Koto 1-1-1, Sayo, Hyogo 679-5148, Japan, [b]Japan Synchrotron Radiation Research Institute, Koto 1-1-1, Sayo, Hyogo 679-5198, Japan, [c]Laboratory of Advanced Science and Technology for Industry, University of Hyogo, Koto 3-1-2, Kamigori, Hyogo 678-1205, Japan, and [d]Department of Material Science, University of Hyogo, Koto 3-2-1, Kamigori, Hyogo 678-1297, Japan. *Correspondence e-mail: ztanaka@spring8.or.jp

Received 20 November 2020
Accepted 28 January 2021

Edited by A. Bergamaschi, Paul Scherrer Institut, Switzerland

Keywords: undulator; tapering.

An undulator generating a magnetic field whose longitudinal profile is arbitrarily varied has been developed, which is one of the key components in a number of proposed new concepts in free-electron lasers. The undulator is composed of magnet modules, each of which corresponds to a single undulator period, and is driven by a linear actuator to change the magnetic gap independently. To relax the requirement on the actuator, the mechanical load on each module due to magnetic force acting from opponent and adjacent modules is reduced by means of two kinds of spring systems. The performance of the constructed undulator has been successfully demonstrated by magnetic measurement and characterization of synchrotron radiation.

1. Introduction

The undulator is an essential component in synchrotron radiation (SR) and free-electron laser (FEL) facilities, which generates a sinusoidal magnetic field and periodically deflects the electron beam. The electromagnetic wave emitted from an electron in the undulator becomes in phase with its motion and thus is intensified at a specific wavelength known as the fundamental wavelength (λ_1). In the typical case when the electron beam energy and magnetic period are constant along the longitudinal (z) axis, λ_1 is defined as

$$\lambda_1(z) = \frac{\lambda_u}{2\gamma^2}\left[1 + \frac{K^2(z)}{2}\right], \tag{1}$$

with

$$K(z) = \frac{eB_p(z)\,\lambda_u}{2\pi mc}, \tag{2}$$

where λ_u is the magnetic period, γ is the Lorentz factor of the electron, e and m are the electron charge and rest mass, respectively, c is the speed of light, B_p is the field amplitude, and K is a dimensionless parameter representing the strength of the magnetic field, which is known as the deflection parameter of an undulator. Note that B_p usually changes randomly along z to some extent, because of a number of factors such as the errors of the magnetization vectors of individual magnets, and deviation in the distance between the top and bottom magnetic arrays (gap, g). This is the reason why B_p is explicitly given as a function of z, and so are K and λ_1. In most applications, the deviation of B_p should be suppressed within some criterion so that λ_1 is kept constant. In general, a lot of effort

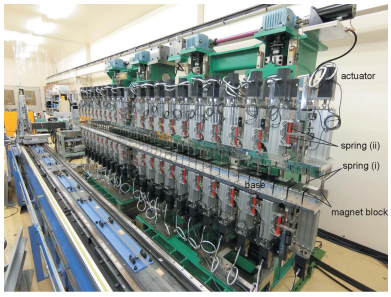

© 2021 International Union of Crystallography

has to be made to eliminate the gap variation along z to guarantee the undulator performance, because B_p strongly depends on g as

$$B_p \propto \exp(-\pi g/\lambda_u). \quad (3)$$

In contrast to the above general application, there exists a special undulator in which g is linearly varied along z to expand the bandwidth of SR. This is referred to as a 'tapered undulator' and is widely used in SR facilities for time-resolved quick-scanning X-ray absorption fine structure techniques (Frahm *et al.*, 2005; Uruga *et al.*, 2007; Nonaka *et al.*, 2012), in which the photon energy can be quickly scanned by a specially designed monochromator based on a channel-cut crystal combined with a servo motor. In X-ray FEL facilities where the undulator is divided into many segments in order to install quadrupole magnets and instruments for diagnostics in between, the gap of each segment is gradually opened from segment to segment to enhance the laser power by compensating for the energy loss of the electron during the lasing process. This scheme is also a kind of undulator tapering.

Besides the applications mentioned above, a number of proposals have been made for a new application of tapered undulators, for the purpose of expanding the possibility of FELs, or manipulating the temporal structure of FEL pulses. For example, a proposal has been made to shorten the pulse lengths available in the so-called high-gain harmonic generation FELs, potentially down to a single-cycle scale (Tanaka, 2015; Kida *et al.*, 2016; Tanaka & Ribič, 2019; Ribič & Tanaka, 2020); the electron beam interacts with a short-pulse seed light in a strongly tapered undulator to form a microbunch, or a density modulation, whose profile is given by a chirped sinusoid (chirped microbunch), which eventually generates short-pulse FEL radiation in the subsequent tapered undulator. Note that, although the undulator tapering in the original proposal is supposed to be linear, it has been shown since that a quadratic or higher-order taper profile may be desirable to fully take advantage of its capability (Goryashko, 2017; Tanaka, 2018; Zhang *et al.*, 2020). Another example is a frequency-modulated FEL (Campbell & McNeil, 2019), in which K is periodically modulated along z and the frequency of the FEL pulse is modulated to generate multiple longitudinal modes that span a much broader bandwidth than conventional FELs.

To demonstrate the above proposals and implement their concepts in FEL facilities, we need a special undulator whose longitudinal magnetic profile $B_p(z)$ can be arbitrarily varied, which is hereafter referred to as a 'VLPU' (variable longitudinal profile undulator). It is easy to imagine that the mechanical and magnetic structures of the VLPU are much more complicated than those of the conventional tapered undulator in which B_p changes linearly. Recently, a VLPU has been constructed to be used in proof-of-principle experiments to demonstrate the chirped-microbunch concept mentioned above. In this paper, we report on the development of the VLPU, together with the results of magnetic measurement and characterization of SR to quantify its performance.

Table 1
Parameters of the VLPU.

Period length	160 mm
Number of periods	24
Minimum gap	40 mm
Maximum K value	10.7

2. Design and construction

The VLPU has been designed to be installed in the NewSUBARU storage ring (Ando *et al.*, 1998), where the electron beam interacts with the seed light to be synchronously injected. Taking into account the boundary conditions such as the electron energy (1 GeV), remanent field of available permanent magnets (1.24 T) and allowable minimum gap (40 mm), λ_u of 160 mm has been chosen, so that λ_1 reaches the wavelength of seed light (Ti:Sa laser, 800 nm). Table 1 summarizes the parameters of the VLPU.

To realize the variable longitudinal profile (VLP) function, the magnetic array is divided into 'magnet modules', each of which is 160 mm (= λ_u) long and can be individually moved along the vertical (y) axis to adjust the local gap $g(z)$ as shown in Fig. 1(*a*), where the magnetic circuit of each module is shown together with the dimensions (in mm) of magnet blocks. Unlike the conventional Halbach configuration, each period is composed of six magnet blocks, two of which are longitudinally magnetized, and the others are vertically magnetized. Note that the former is two times longer than the latter; this is to make sure that each module generates a magnetic field whose profile is symmetric with respect to its center, and the second field integral is ideally zero.

The six magnet blocks (NdFeB, Shin-Etsu Chemical Co., Ltd) are assembled into a module base to form a single undulator period, which is mounted on a pair of linear guides and is connected to a linear actuator (ORIENTAL Motor, DRL60) to allow for the vertical motion to adjust the local gap. The stroke of the actuator is 50 mm, which corresponds to

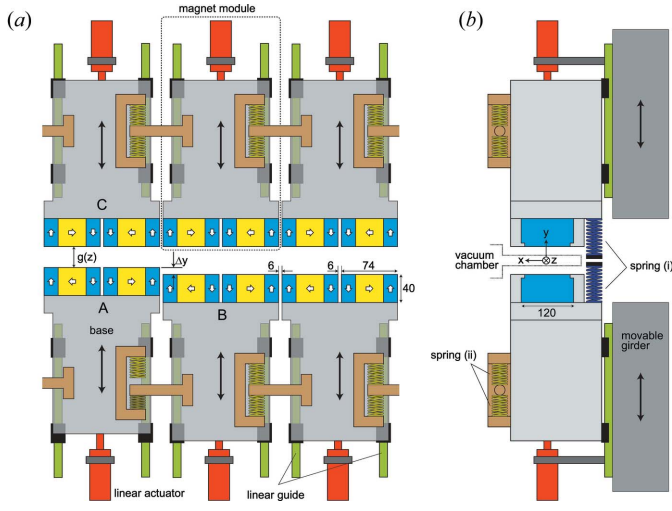

Figure 1
Overall structure of the VLPU: (*a*) side view (three periods) and (*b*) cross-sectional view. See text for details of each element.

the adjustable gap range of 100 mm. We built 48 modules to form a 24-period VLPU and assembled them on the movable girder of an existing undulator mechanical frame, which stopped operation before and has been recycled for construction of the VLPU. The stroke of the movable girder is 120 mm for each module, resulting in the adjustable gap range of 240 mm. Considering the physical constraints, the global gap can be varied from 40 mm to 280 mm with the maximum variation of the local gap of 100 mm as mentioned above. Note that 6 mm-long blank spaces are inserted every other half period; those between adjacent modules are to reduce the magnetic force and facilitate the assembling of each module, while those in the module center are just to keep the symmetry of the magnetic circuit.

Now, let us turn to an important issue which is specific to the developed VLPU, *i.e.* local magnetic force acting on each module. Because of the availability and limited space for installation, the thrust force of the selected actuator is as low as 300 N, and thus the mechanical load acting on each module (including the self weight) should be lower than this value. To reduce the magnetic force, two types of spring systems are attached to the module. The first one (i) is to reduce the attractive force between the top and bottom modules, which is widely used (Marcouille *et al.*, 2010) in conventional undulators. The second one (ii), which is specific to the VLPU, is to reduce the mechanical load acting on a module that is shifted vertically with respect to adjacent ones. The spring constants are 13 and 31 N mm^{-1}, respectively.

For example, let us consider the case when the module A in Fig. 1(*a*) (bottom left) is shifted by the distance of Δy with respect to the module B (bottom middle). Then, the repulsive force between the end magnets in the two modules results in a strong force in the vertical direction acting on both modules A and B. The spring system (ii) works to reduce the mechanical load coming from the vertical displacement between adjacent modules described above.

The parameters of the spring systems (i) and (ii), such as the spring constant and natural length, have been optimized based on numerical studies with the computer code *RADIA* (Chubar *et al.*, 1998) to evaluate the magnetic force and its dependence on the local gap g and vertical displacement Δy. The optimized parameters have been experimentally verified by measuring the mechanical load acting on one of the modules as a function of g and Δy, by means of a load cell inserted between the module base and actuator. The measurement results with and without the spring system are shown in Fig. 2, in terms of the measured force as a function of (*a*) g and (*b*) Δy. For reference, the computed results without the spring system are also shown. In both conditions, the mechanical load is suppressed well below 300 N (thrust force of the actuator).

In the VLPU design described above, a spring-based approach has been taken to reduce the magnetic force acting on the modules. Although the requirement on the actuator is significantly relaxed, we have two issues to be improved for the future development. First, the attractive force between the top and bottom modules is not completely eliminated as found in Fig. 2(*a*). Second, the spring system (ii) imposes a physical limit on the movable range of the vertical displacement Δy. An alternative method to overcome these difficulties is to make use of additional magnet arrays on both sides of the main magnets (Kinjo *et al.*, 2017) as illustrated in Fig. 3, where the phase of the additional magnet is adjusted to reduce the attractive force between the top and bottom modules and the repulsive forces between adjacent ones.

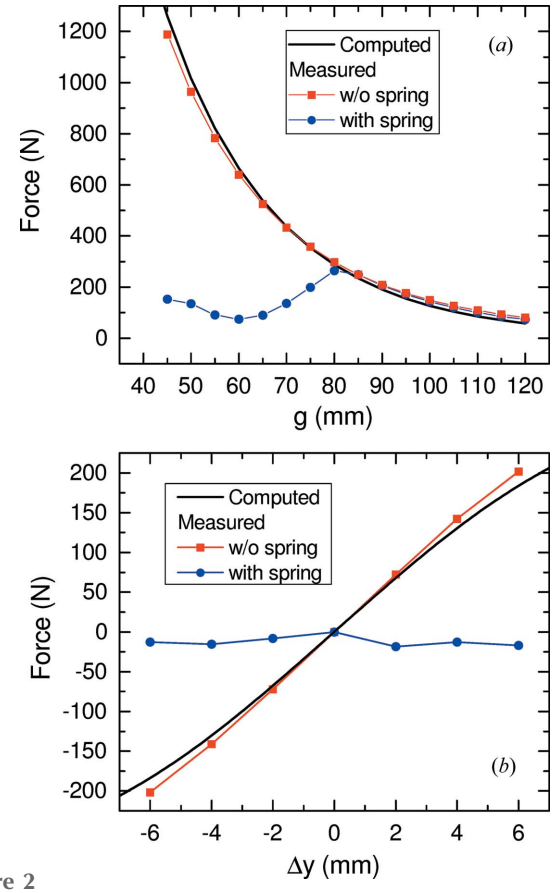

Figure 2
Mechanical load acting on a single magnet module as a function of (*a*) g and (*b*) Δy, measured with and without the optimized spring system. Computed results without the spring systems are also shown.

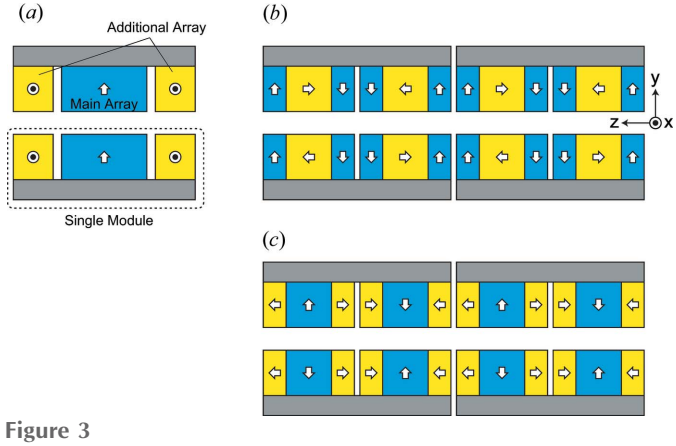

Figure 3
Schematic drawing of additional magnetic arrays to reduce the magnetic force: (*a*) cross-sectional view, (*b*) side view of the main array and (*c*) side view of the additional array.

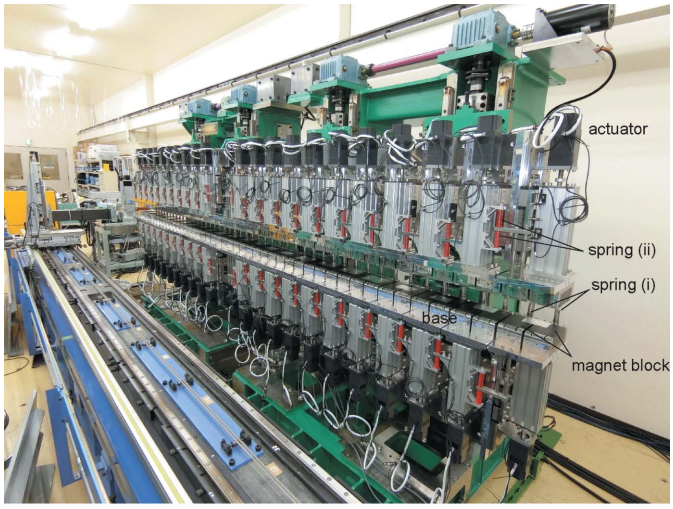

Figure 4
Photograph of the VLPU during the process of magnetic measurement.

3. Experimental demonstration

After assembling all the modules and other components, the performance of the VLPU has been examined by means of magnetic measurement and characterization of SR, the results of which are reported in this section. Fig. 4 shows a photograph of the developed VLPU during the magnetic measurement.

3.1. Magnetic measurement

It is well known that the quality of an undulator is represented by two types of errors, the integrated multipole and phase error, which should be corrected as much as possible. In the development of the VLPU, the former was corrected by putting a number of shim plates on the surface of the magnet blocks, which is a typical method in conventional undulators. In contrast, the correction of the latter was carried out in a more efficient manner, by taking advantage of the VLP function; the vertical displacement Δy of each module was optimized to reduce the phase error, which can be easily done by analyzing the measured field profile. Fig. 5(*a*) shows the result of correction, in which the phase error evaluated from the measured field profile is plotted as a function of z, before (initial, dotted line) and after (solid line) the optimization. The RMS phase error is reduced from 14° to 2.5°, which is low enough for most applications, and is preserved in the working gap range (less than 3° from 40 to 140 mm).

It is worth noting that the above result has been achieved just after a few cycles of measuring the field profile and analyzing the result for optimization, which is much faster than the process of phase-error correction in conventional undulators. The maximum displacement Δy for the phase-error correction was of the order of 0.3 mm, and the second

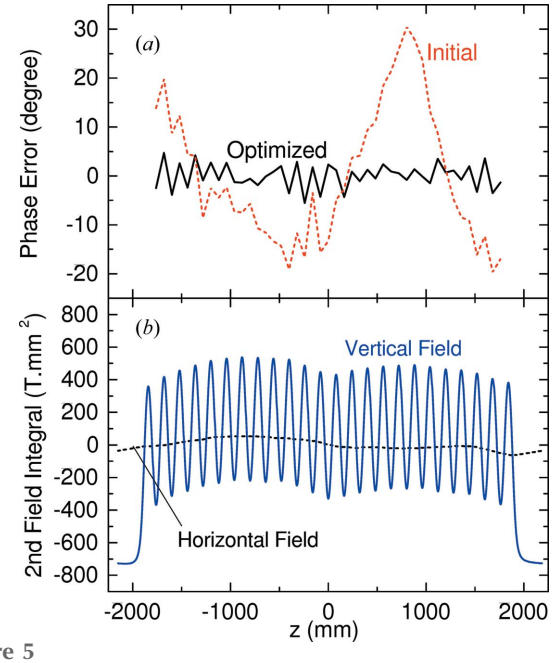

Figure 5
(*a*) Phase errors and (*b*) second field integrals evaluated from the magnetic field profile measured after assembling (dotted line) and optimization of Δy (solid line).

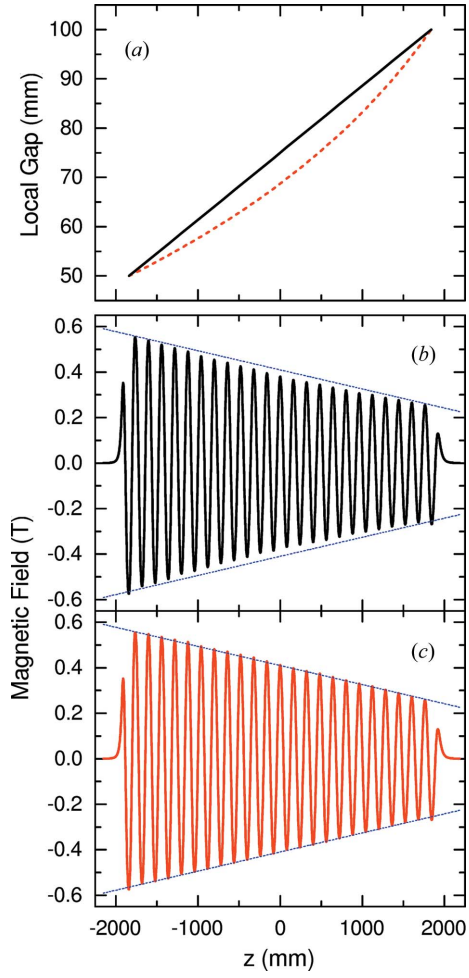

Figure 6
Example of linearizing the field profile. The solid line in (*a*) shows a linear gap variation with the measured field profile shown in (*b*), while the dashed line in (*a*) shows an adjusted gap variation for linearization with the measured profile shown in (*c*). Note that the dotted lines in (*b*) and (*c*) indicate linearly decaying envelopes.

field integral (electron orbit) shown in Fig. 5(*b*) was hardly changed by the vertical displacement.

Another important function of the VLPU is to generate an arbitrary field profile, which is the original motivation for its development. As an example, we examined the possibility to generate a field profile whose amplitude linearly changes with a large gradient. The most straightforward way is to change the local gap linearly, as shown by the solid line in Fig. 6(*a*), from 50 to 100 mm in this example. The magnetic field profile measured in this condition is shown in Fig. 6(*b*). Roughly speaking, the field amplitude changes linearly; however, the deviation from the linear function (dashed lines) is not negligible around the center ($z = 0$). This is attributable to the exponential dependence of the magnetic field on the gap as given in equation (3). To correct the deviation, $g(z)$ was modified using this formula so that the resultant field variation becomes linear, which is shown by the dashed line in Fig. 6(*a*). The field profile measured under this condition is shown in Fig. 6(*c*), where the field amplitude changes completely linearly as expected.

Note that the local gap adjustment to linearize the field profile, as reported in the above example, is not usually needed in most applications, in which the gap variation is relatively small compared with the magnetic period. This is easily understood by recalling equation (3). Even so, the above example demonstrates well the capability of the developed VLPU.

3.2. Characterization of SR

Having verified the performance based on the magnetic measurement, the VLPU has been installed in BL01 of the NewSUBARU storage ring. For characterization of SR, we measured spectra with a fiber-coupled multichannel spectrometer (AVANTES, Avaspec-ULS2048L-USB2) located 22 m far from the center of the VLPU. The active area of the spectrometer is 0.4 mm in diameter, corresponding to an acceptance angle of 0.018 mrad. This is much narrower than the angular divergence of SR and thus the measured spectra correspond to the on-axis flux.

The spectral measurements were carried out for five different conditions of magnetic profile (i)–(v), which are indicated by the local gap variation $g(z)$ as shown in Fig. 7(*a*); condition (i) refers to a constant profile at the gap of 63 mm (with the nominal K value of 6.7), while (ii), (iii) and (iv), (v) refer to linear and parabolic profiles, respectively. Note that corresponding peak-field variations are plotted in Fig. 7(*b*) for reference. The measurement results are plotted in Fig. 7(*c*), which are normalized by the maximum spectral intensity given in the condition (i). To examine the validity of these results, we numerically computed the spectra under respective conditions using the computer code *SPECTRA* (Tanaka & Kitamura, 2001), with the electron beam parameters in BL01 of NewSUBARU taken into account (which are summarized in Table 2). The results are shown in Fig. 7(*d*), which are in good agreement with the experimental ones. It is worth noting that the spectral oscillation as found in the conditions (iv) and (v) has been analyzed in a previous paper (Brau, 2004).

Table 2
Electron beam parameters in BL01 of the NewSUBARU storage ring.

Electron energy	1.0 GeV
Natural emittance	37 nm rad
Coupling constant	0.01
Energy spread	4×10^{-4}
Horizontal betatron function	1.49 m
Vertical betatron function	8.05 m

4. Summary

We presented the development of a new undulator referred to as a 'VLPU', in which the local gap can be adjusted at each period with an actuator assisted by spring systems to reduce the mechanical load. In contrast to conventional undulators, the VLPU can generate a magnetic field profile that is fully variable, and we successfully demonstrated its performance through the magnetic measurement and characterization of SR. As mentioned in Section 1, the VLPU is expected to be a key component of special FEL schemes such as the chirped-microbunch concept.

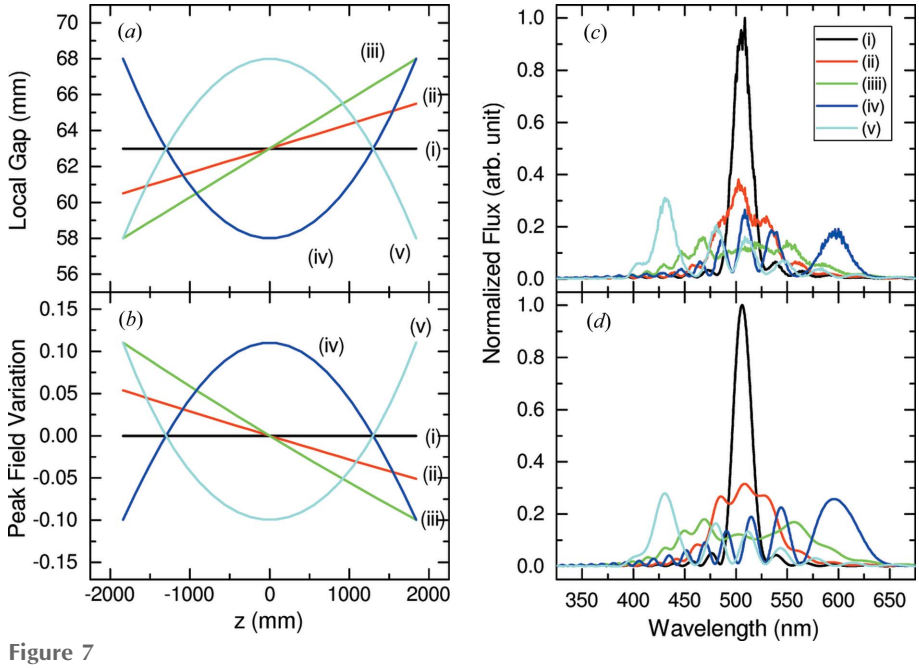

Figure 7
(*a*) Five different conditions of the local gap variations examined in the spectral measurement, and (*b*) corresponding peak field variations. (*c*) Measured and (*d*) computed spectra of SR under the five conditions.

Finally, we mention the applicability of the VLPU design presented in this paper, where a pure permanent magnet configuration with a relatively long period (160 mm) has been chosen. Obviously, the design can be applied to the so-called hybrid configuration, in which pole pieces made of a high-permeability material are inserted between permanent magnets. In contrast, the available period depends on the capability and dimension of the actuator: a longer/shorter period requires a more powerful/smaller actuator.

Acknowledgements

The authors thank Mr Seike of Japan Synchrotron Radiation Research Institute for supporting the construction and installation of the VLPU.

Funding information

Funding for this research was provided by: Japan Society for the Promotion of Science (JSPS) (grant No. KAKENHI JP18H03691).

References

Ando, A., Amano, S., Hashimoto, S., Kinosita, H., Miyamoto, S., Mochizuki, T., Niibe, M., Shoji, Y., Terasawa, M., Watanabe, T. & Kumagai, N. (1998). *J. Synchrotron Rad.* **5**, 342–344.
Brau, C. A. (2004). *Phys. Rev. ST Accel. Beams*, **7**, 020701.
Campbell, L. T. & McNeil, B. W. J. (2019). *Opt. Express*, **27**, 8792–8799.
Chubar, O., Elleaume, P. & Chavanne, J. (1998). *J. Synchrotron Rad.* **5**, 481–484.
Frahm, R., Richwin, M. & Lützenkirchen-Hecht, D. (2005). *Phys. Scr.* **115**, 974.
Goryashko, V. A. (2017). *Phys. Rev. Accel. Beams*, **20**, 080703.
Kida, Y., Kinjo, R. & Tanaka, T. (2016). *Appl. Phys. Lett.* **109**, 151107.
Kinjo, R., Kagamihata, A., Seike, T., Kishimoto, H., Ohashi, H., Yamamoto, S. & Tanaka, T. (2017). *Rev. Sci. Instrum.* **88**, 073302.
Marcouille, O., Bechu, N., Brunelle, P., Berteaud, P., Chapuis, L., Couprie, M.-E., Filhol, J.-M., Herbeaux, C., Lestrade, A., Marlats, J.-L., Massal, M., Mary, A., Nguyen, M., Tavakoli, K., Valleau, M. & Veteran, J. (2010). *Proceedings of the First International Particle Accelerator Conference (IPAC2010)*, 23–28 May 2010, Kyoto, Japan, pp. 3102–3104.
Nonaka, T., Dohmae, K., Araki, T., Hayashi, Y., Hirose, Y., Uruga, T., Yamazaki, H., Mochizuki, T., Tanida, H. & Goto, S. (2012). *Rev. Sci. Instrum.* **83**, 083112.
Rebernik Ribič, P. & Tanaka, T. (2020). *Opt. Lett.* **45**, 5234–5237.
Tanaka, T. (2015). *Phys. Rev. Lett.* **114**, 044801.
Tanaka, T. (2018). *Opt. Lett.* **43**, 4485–4488.
Tanaka, T. & Kitamura, H. (2001). *J. Synchrotron Rad.* **8**, 1221–1228.
Tanaka, T. & Rebernik Ribič, P. (2019). *Opt. Express*, **27**, 30875–30892.
Uruga, T., Tanida, H., Inoue, K., Yamazaki, H. & Irie, T. (2007). *AIP Conf. Proc.* **882**, 914–916.
Zhang, H., Wang, W., Jiang, S., Li, C., He, Z., Jia, Q., Wang, L. & He, D. (2020). *Phys. Rev. Accel. Beams*, **23**, 020704.